X-ray forward diffraction wave-front propagation in Si and C single crystals: Simulations and experiments

A. Rodriguez-Fernandez[*,a], G. Carbone[b], Z. Matej[b], D. Grolimund[c], D. F. Sanchez[c], and B. Pedrini[c]

[a]European XFEL GmbH, Holzkoppel 4, Schenefeld DE-22869, Germany
[b]MAX IV Laboratory, Lund University, Fotongatan 2, Lund Se-22100, Sweden
[c]Paul Scherrer Institute, Forschungsstrasse 111, Villigen PSI CH-5232, Switzerland

ABSTRACT

The emergence of new high brilliance and high coherence facilities such as X-ray Free Electron Lasers (XFELs) and 4^{th} generation synchrotrons open a new era in X-ray optics. Dynamical diffraction effects before disregarded are starting to play a role in the beam control of large scale facilities. In the case of XFEL facilities the temporal characteristics of the dynamical diffraction by thin perfect crystals can be used as a tool to generate femtosecond monochromatic pulses, in the case of self-seeding in the hard X-ray regime, but could even be used as method to characterize materials in this temporal range. In this contribution we present the first steps in the understanding of the spatial-displacement dependence of forward beams diffracted by thin crystals. The data collected by this technique is compared with crystal models based in dynamical diffraction theory. This type of study could open a new field to understand low strain materials in the femtosecond regime.

Keywords: Dynamical Diffraction theory, Forward diffraction, X-ray thin optics

1. INTRODUCTION

With the proliferation of new high brilliant sources as X-ray Free Electron Lasers (XFEL) and 4^{th} synchrotron ring sources a new range of X-rays physics is opening.[1,2] The transversal and longitudinal coherence are starting to play a role in the design of X-ray optics for these new sources. The high coherence couples with the perfection of the crystals commonly used as optics to collimate, attenuate, monochromatize or diagnose the X-ray beams. Dynamical diffraction effects have been previously studied as temporal independent effects, so called standing waves, in perfect crystals. The new sources, and in particular XFEL facilities, reveal the temporal length of these processes. This is of particular interest at XFELs, where the dynamical diffraction length in thin perfect crystals is of the order of the femtosecond or even the hundreds of attoseconds. This temporal dependence relates to the energy of the X-rays and crystal parameters such as chemical composition, thickness or crystal cut.

Conventionally XFELs present X-ray bandwidth of the order of 10 to 30 eV due to the self-amplified spontaneous Emission (SASE) process which generates the radiation. This bandwidth depends on the stochastic shot-to-shot noise of the machine. To improve the energy resolution the use of a monochromator in between undulartor sections, the so called Self-Seeding (SS), was proposed.[3] A particular case is forward SS, first proposed by Geloni and co-workers.[4] Forward beam SS is a dynamical diffraction based technique, that uses thin perfect diamond crystals as temporal monochromators. SS has shown to be able to reduce the bandwidth to 1 eV, similar to the case of Si (111) monochromator, and improves stability shot-to-shot. SS has been implemented at different XFELs sources and is under commissioning at the European XFEL.[5]

Thin single crystals are not only used at hard XFEL facilities for self-seeding, but also for many different X-ray diagnostics and X-ray optics instrumentation such as spectrometers, monochromators or attenuators. In particular, in the case of spectrometers and monochromators the effects of dynamical diffraction can disturb the propagation of the X-ray beam. But even in the case of the attenuators, for some specific energies and surface orientations, non symmetric Laue reflections in could be excited.[6]

Further author information: (Send correspondence to A.R.F.)
A.R.F.: E-mail:angel.rodriguez-fernandez@xfel.eu, Telephone: +49 40 8998 6801

Advances in Computational Methods for X-Ray Optics V, edited by Oleg Chubar, Kawal Sawhney, Proc. of SPIE Vol. 11493, 114930W · © 2020 SPIE
CCC code: 0277-786X/20/$21 · doi: 10.1117/12.2568495

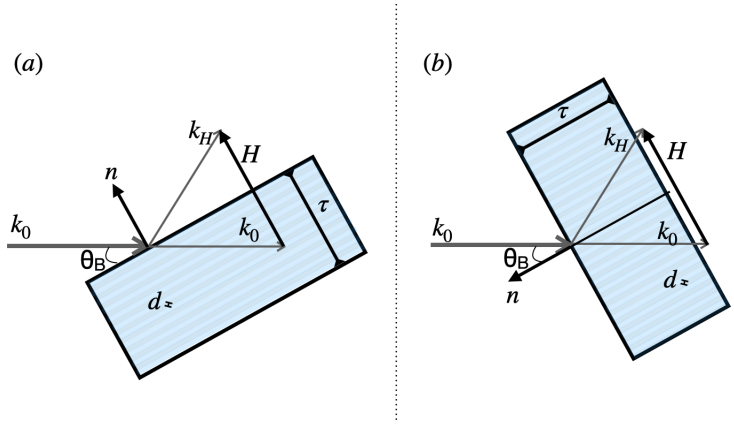

Figure 1. Sketch of the diffraction geometry from a thin crystal for both (a) Bragg and (b) Laue co-planar geometry. The reciprocal lattice vector **H** and the surface normal **n**, are represented in black. The crystal of thickness τ is indicated with a bounded black line. The diffraction planes of spacing d are represented with stripes parallel lines. The wave vector of the incident and transmitted beam is $\mathbf{k}_0$, while that for the diffracted beam is $\mathbf{k}_H$. The incident angle at the diffraction condition, θ_B, is indicated.

In the case of MHz repetition rate sources as the European XFEL, Si based X-ray optics can suffer thermal expansion effects between photon pulses. This thermal expansion in the case of monochromators can change both the intensity of the transmitted pulse and also the energy bandwidth of the photons. Diamond shows much better thermal properties making them ideally suited for MHz XFELs. But the production of thick defect-free crystals is expensive and difficult. For these two reason thin crystals are usually used. Thin crystals however lead to dynamical diffraction femtosecond processes as the ones presented in this proceeding both in the diffracted and forward beams.

In this proceeding, we present both experimental and simulations studies of the dynamical diffraction effects observed in the forward direction for diamond, C, and silicon, Si, thin crystals, as also presented in our previous Rodriguez-Fernandez et al.[7] The experiment were performed at MicroXAS beamline of the Swiss Light Source. To enhance the spatial resolution a set of KB mirrors with a foci of 2 μm were used. Also this beamline is capable of a high energy resolution, which is perfect for the imaging of dynamical diffraction effects in thin single crystals.

2. THEORY

The geometries under consideration are presented in Figure 1. An incoming X-ray wave, $\mathbf{k_0}$, hits a medium with periodic susceptibility, $\chi(r)$, and infinite transverse extension.

$$\chi(r) = \sum_H \chi_H e^{-2\pi i \mathbf{H}\cdot\mathbf{r}} \quad , \tag{1}$$

If the crystal is oriented such as a family of atomic planes is set to diffraction condition, the incident beam will be partially diffracted, both in the diffraction direction, $\mathbf{k_H}$, and in the forward direction, $\mathbf{k_0}$. The precise redistribution of the beam intensity between transmitted and diffracted directions depends mainly on the energy and bandwidth of the incoming beam, as well as the geometry of the diffraction and the thickness of the crystal. This redistribution of the intensity can be described with dynamical diffraction theory and relates to the excitation of the two diffraction branches α and β of diffraction for the excited reflection.

In the geometry under consideration the incident wave vector $\mathbf{k_0}$, the reciprocal lattice of the crystal reflection and the surface unit normal **n** are restricted to lie in the same plane, corresponding to the drawing plane of figure 1. The incoming beam is defined by the wave vector k, which is related to the photon wavelength λ by $k = 2\pi/\lambda$. The diffraction vector is defined by $H = 2\pi/d$, where d is the plane spacing of the corresponding reflection. The angle between $\mathbf{k_0}$ and $-\mathbf{H}$ correspond to the incidence angle $90 - \theta$, and **H** and $-\mathbf{n}$ define the

asymmetry angle of the reflection to the surface of the crystal, δ. The Bragg condition of diffraction is written as

$$\mathbf{k_0} - \mathbf{k_H} = \mathbf{H} \quad , \tag{2}$$

which defines for a given photon energy the Bragg angle θ_B. In the case of a elastic process, as consider here, the wave vector of the diffracted $\mathbf{k}_H$, diffracted forward $\mathbf{k}_0$ and transmitted waves have the same length k. And its direction is uniquely defined by requiring that the difference vector $(\mathbf{k}_H - (\mathbf{k}_0 + \mathbf{H}))$ is parallel to $\mathbf{n}$.[8] The wave vector of the diffracted forward plane wave is the same as that of the incident wave. Other parameters of the crystal that are relevant for the diffraction process are the crystal thickness τ, the unit cell volume V, and the Fourier transform of the unit cell structure factors F_0, F_H and $F_{\bar{H}}$, where $\bar{\mathbf{H}}$ is $-\mathbf{H}$, the inverse reciprocal lattice.

We define a electric displacement field inside the crystal by

$$\mathbf{D}(\mathbf{r}) = \sum_H \mathbf{D_H} e^{-2\pi i \mathbf{k_H}\cdot\mathbf{r}} \quad , \tag{3}$$

When performing the sum over all the Fourier components in the reciprocal lattice vectors H, the fundamental equation of dynamical theory is obtained:[8,9]

$$\sum_H \chi_{H-\bar{H}}[(\mathbf{k_H}\cdot\mathbf{D_{H'}})\mathbf{k_H} - k_H^2\mathbf{D_{H'}}] = (k^2 - k_H^2)\mathbf{D_H}. \tag{4}$$

The diffraction process is a two beam problem, this simplifies the problem to

$$\begin{aligned} \chi_{\bar{H}}[(\mathbf{k_0}\cdot\mathbf{D_H})\mathbf{k_0} - k_0^2\mathbf{D_H}] &= [k^2 - k_H^2(1-\chi_0)]\mathbf{D_0} \\ \chi_H[(\mathbf{k_H}\cdot\mathbf{D_0})\mathbf{k_H} - k_H^2\mathbf{D_0}] &= [k^2 - k_H^2(1-\chi_0)]\mathbf{D_H}, \end{aligned} \tag{5}$$

where $\mathbf{D_H}$ and $\mathbf{D_0}$ are the displacement field in the diffraction and incoming directions. These vector equations define the physical possible values for $D_{0,H}$ and it can be solve to retrieve the diffracted and forward beam amplitudes. The system of consist in four equations, two for each surface. In the case of the front or incoming surface:

$$\begin{pmatrix} D_0 \\ D_H \end{pmatrix}^{(front)} = \begin{pmatrix} 1 & 1 \\ c_1 & c_2 \end{pmatrix} \begin{pmatrix} D_1 \\ D_2 \end{pmatrix}^{(cryst)} \quad , \tag{6}$$

and for the rear surface

$$\begin{pmatrix} D_0 \\ D_H \end{pmatrix}^{(rear)} = \begin{pmatrix} \Upsilon_1 & \Upsilon_2 \\ c_1\Upsilon_1 & c_2\Upsilon_2 \end{pmatrix} \begin{pmatrix} D_1 \\ D_2 \end{pmatrix}^{(cryst)} \quad , \tag{7}$$

here the values D_1 and D_2 define the field inside the crystal, and i denotes the nth layer in the crystal. For the solution of this system of equations we can obtain the coefficient of reflection R and transmission T for the process.

For a crystal in Bragg geometry (Figure 1(a)), in which the diffracted wave is emerging from the same crystal surface as the incoming wave ($-\theta_B < \delta < \theta_B$). The boundary condition in the rear surface impose that the diffraction wave D_H^2 should be 0 and D_0^0 is the incoming beam that we can consider as 1. These leaves two variables to be solved $R = D_H^0$ and $T = D_0^2$:

$$T(k,\theta) = \frac{c_1 c_2(\Upsilon_2 - \Upsilon_1)}{c_2\Upsilon_2 - c_1\Upsilon_1} \quad , \quad R(k,\theta) = \frac{\Upsilon_2\Upsilon_1(c_1 - c_2)}{c_2\Upsilon_2 - c_1\Upsilon_1} \quad . \tag{8}$$

In the case of Laue geometry the diffracted wave is emerging by the same crystal surface as the transmitted wave ($\theta_B < \delta$), this sets boundary condition in the incoming surface were D_H^0 should be 0 and D_0^0 equal to 1. If we solve the system of equation with these conditions we obtain $R = D_H^2$ and $T = D_0^2$:

$$T(k,\theta) = \frac{(c_1\Upsilon_2 - c_2\Upsilon_1)}{\Upsilon_2 - \Upsilon_1} \quad , \quad R(k,\theta) = \frac{\Upsilon_2\Upsilon_1(c_1 - c_2)}{\Upsilon_2 - \Upsilon_1} \quad . \tag{9}$$

The expressions appearing in the above formulas are

$$\Upsilon_{1,2} = \frac{-\eta \pm \sqrt{s+\eta^2}}{P\psi_{\bar{H}}} \quad , \quad c_{1,2} = e^{-i\varphi_{1,2}\tau}, \quad \varphi_{1,2} = \frac{k_0}{2\gamma_0}(\psi_0 - \eta \pm \sqrt{s+\eta^2})$$

where the index $1, 2$ related to the $+, -$ signs, respectively, P is the polarization of the X-ray, which is 1 for σ and $cos(2\theta)$ for π, and

$$\eta = \frac{1-b}{2}\psi_0 + \frac{b}{2}\alpha \quad , \quad s = b\psi_H\psi_{\bar{H}} \quad ,$$

with $\psi_q = -F_q \cdot (4\pi r_e)/(V\,k^2)$ for $q = 0, H, \bar{H}$, where F_q is the structure factor of the crystal for the reflection understudy. The b

$$b = (1 + \frac{\mathbf{n}\cdot\mathbf{H}}{\mathbf{n}\cdot\mathbf{k_0}})^{-1} \approx \frac{\gamma_0}{\gamma_H} \quad ,$$

here γ_0 and γ_H denote the direction cosine of the incoming and diffracted beam. And α is

$$\alpha = \frac{1}{k^2}(H^2 + 2\mathbf{H}\cdot\mathbf{k}_0) \approx 2\sin(2\theta_B)(\theta_B - \theta) \quad ,$$

The two last approximations are valid for small differences $\theta_B - \theta$.

As discussed in Ref (7), we are considering X-ray beams with small divergence and a finite transverse extension. These X-ray beams can be described in the Fourier space approach by defining a set of spatial coordinates (x, y, z), where z is the coordinate along the beam propagation, x is the transverse coordinate in the diffraction plane, and y is define perpendicular to the diffraction process. A beam is then defined by specifying the Fourier components of the electric field $\hat{E}(k, k_x, k_y, z)$ at any longitudinal point z, from which the field on the corresponding transverse plane and as a function of time is obtained by Fourier transformation

$$E(t,x,y,z) = \int dk\, dk_x\, \hat{E}(k,k_x,k_y,z)e^{-i2\pi(ckt - k_x x - k_y y)} \quad . \tag{10}$$

It is here important to remark that amplitude and phase of the electric field in the transmitted beam is independent from the position of the crystal along the beam propagation direction. Indeed, the free space propagator and the through-crystal propagator commute as presented in Ref(7). This means that the total intensity of the diffracted beam is independent on the crystal z-position.

When a short pulse propagates through a perfect thin crystal oriented to generate a diffracted beam, one observes beats of X-ray intensity that are delayed with respect to the main high-intensity pulse.[4,10] The spatio-temporal coupling is related to the superposition of photon energies ck and the transverse wave vector components k_x. These beats have been called temporal echoes. In the same way, when a monochromatic X-ray beam of narrow waist traverses the crystal, part of the X-ray intensity is displaced transversely and appears as lateral humps, called spatial echoes, in a near field image at the beam waist.[11–13]

The time delay and the transverse displacement associated to an echo are related linearly by

$$\Delta x = c\cot(\theta)\Delta t \quad , \tag{11}$$

see Figures 6 and 9 of Ref.(10).

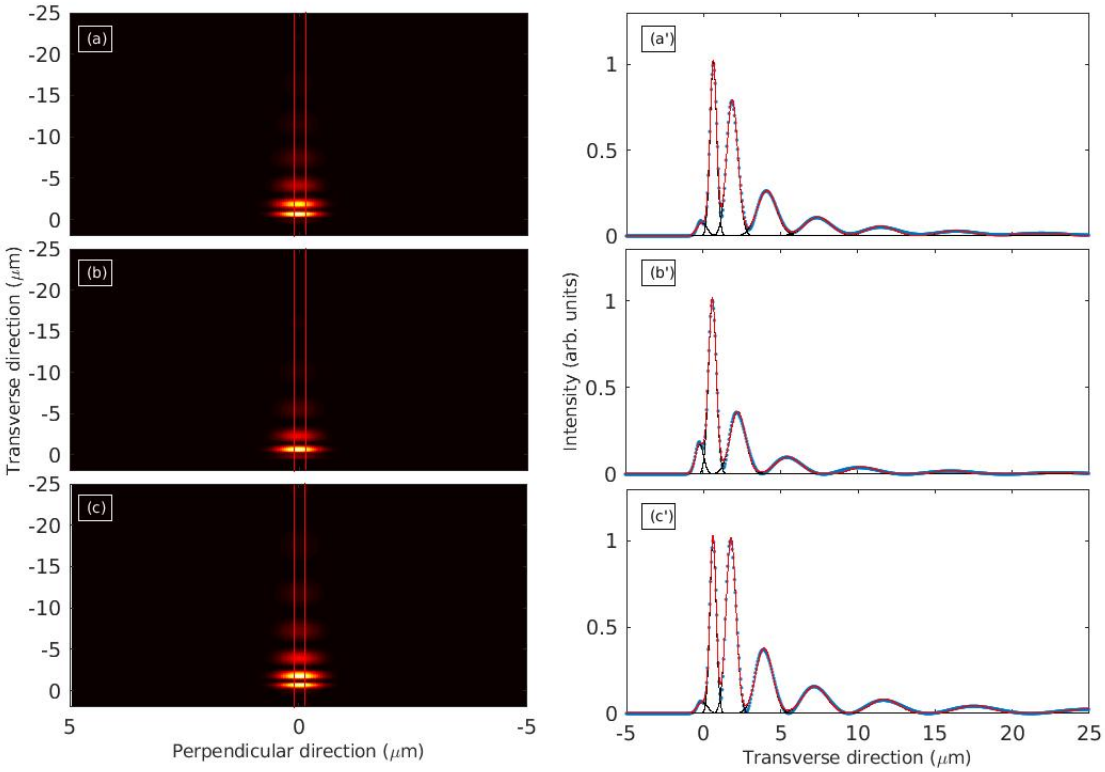

Figure 2. (Left) Simulated forward intensity in the detector plane (x) and (Right) fitted projection along the transverse direction to diffraction (x') for three thin crystals at $9.4keV$: (a) Si (400) reflection in Bragg geometry, (b) C (400) reflection in Bragg geometry and (c) C (022) reflection in Laue geometry. The simulated crystal had a thickness of 100 μm and 220 μm for Si and C, respectively. The red

3. SIMULATIONS

We performed simulations for the configurations that were measured experimentally. The simulations were performed in forward geometry for an energy of 9.4 keV The width of the intensity profile of the beam at the waist was set to the FWHM value $2\sqrt{\ln 2}\sigma_x = 1$ μm. This was set intentionally smaller than the experimental beam size at MicroXAS which improves the spatial resolution of the simulated data for the discussion. The Darwin width of the incoming beam for the simulations is defined by a $Si(311)$ crystal, as in the experimental example. It must be pointed out that the spectra and temporal shapes assumed for the incoming X-ray pulses are not realistic for synchrotron or SASE-FEL X-ray sources, but are simplified in the simulation.

Figure 2 presents the time integrated echo signal for the three simulated cases at the diffraction condition. (a) A Si crystal of thickness $\tau = 100$ μm was assumed in symmetric Bragg geometry for the (400) reflection, (b) a diamond crystal of thickness $\tau = 220$ μm was assumed for a symmetric Bragg geometry for the reflection (400), as well as (c) for a symmetric Laue geometry for the (022) reflection.

To analyse the location and intensity of each of the echoes a multiple Gaussian peak function was used of the form

$$S^{\text{fit}}_{\text{Gauss}}(x) = \sum_{i=0}^{N_e} \frac{A_i}{\varpi_i} e^{-\frac{1}{2}(\frac{x-x_i}{\varpi_i})^2} \quad . \tag{12}$$

N_e is the number of echoes that are considered for the modeling. The parameters x_i, w_i and A_i are the position, the r.m.s. width and the integrated signal of the i-th echo. The full width at half maximum is given by FWHM=$2\sqrt{2\ln 2}$ ϖ_i.

4. EXPERIMENT

Two samples a Si (100) oriented thin crystals of $100\mu m$ thickness and a diamond (100) oriented of $220\mu m$ thickness were studied in Bragg geometry for the (400) reflection. For the diamond crystal also a Laue reflection (022) was studied.

The selection of the beamline was done in relation of the key parameters for this experiment, photon energy, foci at the detector position (to improve spatial contrast) and bandwidth to match the reflections under study. Thus the Si(311) two-bounce monochromator and the two bendable Kirckpatrick-Baez (KB) mirrors at MircorXAS are ideally suited. The focusing was set to $1.5(v) \times 1.0(h)$ μm FWHM at the detector plane, 100 mm distance downstream of the mirror box. The vertical divergence of the focused beam was reduced as much as possible by closing the vertical slits upstream of the KB mirror box. At the focal position a X-ray microscope was located. This microscope consists of a YAG:Ce scintillator crystal, a optical magnification of 40x and a sCMOS pco.2000 aircolled ($6.5\mu m/pixel$). The theoretical resolution of the system is 0.166 μm. The diffracted intensity was observed using an Eiger 500 K detector, located at the 2θ angle for each of the reflections under study. To perform the data collection, each individual single crystal was mounted on a vertical rotation stage with a precision of 0.0005°, located in the path in between the KB mirror exit and the detector. Implicit in this procedure is that we targeted only reflections with vertical diffraction geometry with σ-polarization.

An energy scan of 8 eV was perform around of the reflection with 0.3 eV resolution. At each of the energy positions 5 images, each with $0.2s$ exposure, were recorded with the forward area detector to avoid saturation. The 5 images were then added up to obtain a single image.

Figure 3 present two images for each of the reflections under study. One 3 eV away of the diffraction condition and a second one at the diffraction condition where echoes appear. The location of the echoes depend on the reflection, geometry and element understudy.

5. DISCUSSION AND RESULTS

Figure 4 presents the analysis of the images collected as presented above. For each reflection three energies were selected, -3 eV, 0 eV and 3 eV with respect to the diffraction condition. In each of this images, a section with $1\mu m$ width was cropped and integrated along the perpendicular direction of the detector. In this way the profile of the diffraction along the transverse direction was obtained.

In analogy to the fitting procedure for the simulated data basing on Eq. (12), the echo signals were modeled with the function

$$S^{\text{fit}}_{\text{Lorentz}}(x) = \sum_{i=0}^{N_{\text{echoes}}} \frac{A_i}{\omega_i} \frac{1}{1 + \frac{(x-x_i)^2}{\omega_i^2}} + C_{\text{bg}} \quad . \tag{13}$$

Instead of Gaussians, Lorentzian peak shapes were used to account for the broader peak base, which was observed even without a crystal placed in the beam.

Using eq 13 to fit the profiles in figure 4, we observed that the profile of the beam along the transverse direction can be fitted with a single Cauchy distribution far from the diffraction condition. While at the diffraction condition, the profile must be described with several distributions with their center distributed along the transverse direction.

Figure 5 presents the comparison between the position of the forward diffracted beams for experimental and simulated data. the position 0 in both axis represents the main transmitted beam, this position was fitted at an energy of 3 eV away of the diffraction condition. The position of the maxima close to the transmitted beam is in good agreement with the simulated positions and deviates slightly with increased distance, both Bragg geometry cases $x = 0.95y$. This could be related to a missalignment in the optical microscope. In the Laue case,the slope could be related to a misalignment of the plane with respect to the diffraction plane due to the precision in the manual alignment of the sample as also discussed in Ref.(7).

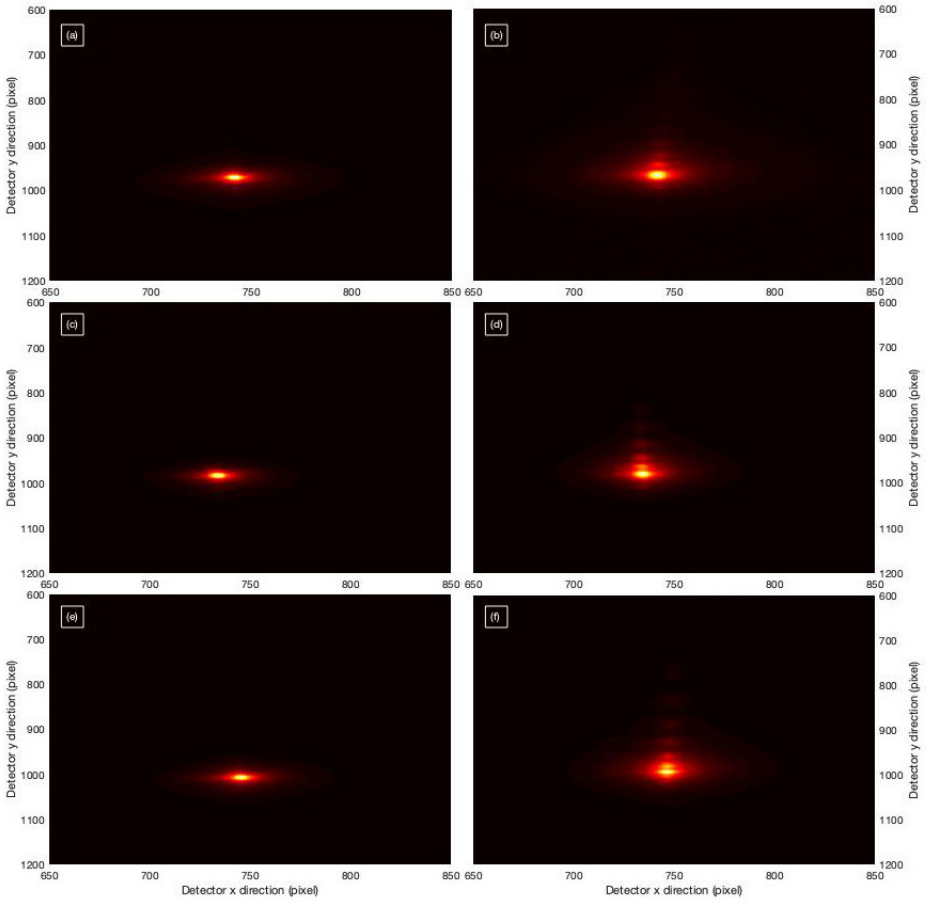

Figure 3. Collected images of the transmitted beam in the forward direction for three thin crystals at $9.4keV$ at MicroXAS beamline. (a) 3 eV away and (b) at the condition of diffraction for Si (400) reflection in Bragg geometry, (c) 3 eV away and (d) at the condition of diffraction for C (400) reflection in Bragg geometry and (e) 3 eV away and (f) at the condition of diffraction for C (022) reflection in Laue geometry. The crystal under studied had a thickness of 100 μm and 220 μm for Si and C, respectively.

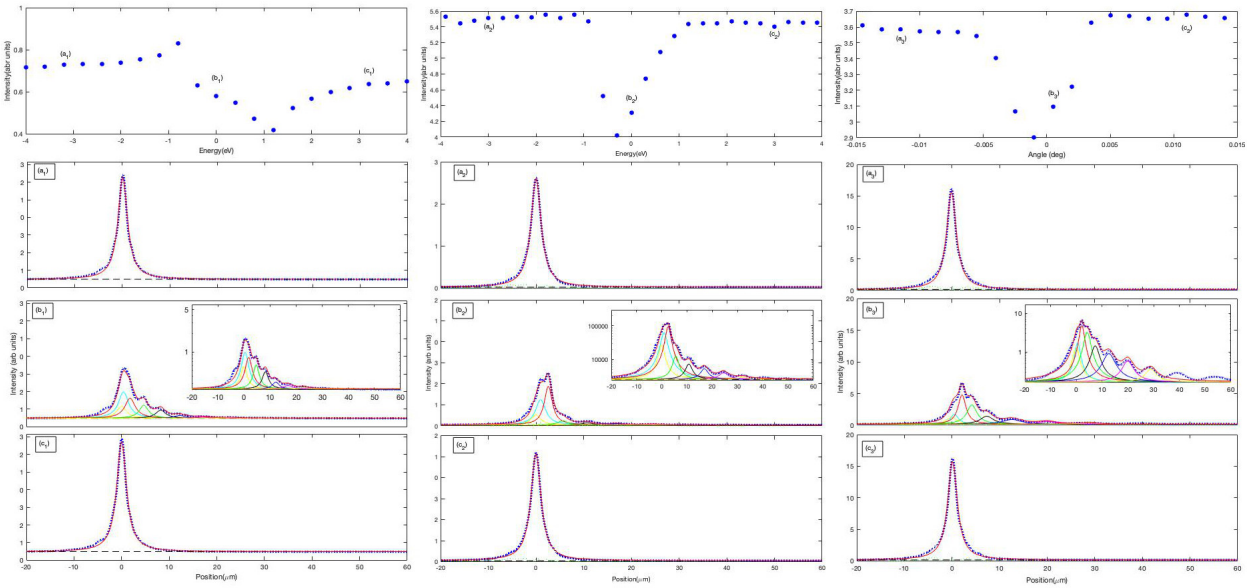

Figure 4. (Top) energy scan perform for each of the three samples (a) Si (400) reflection in Bragg geometry, (b) C (400) reflection in Bragg geometry and (c) C (022) reflection in Laue geometry. Fit to a section $1\mu m$ along the transverse direction for the image presented in Figure 3 at three position of the energy scan. (x_1) $-3eV$, (x_2) $0eV$ and (x_3) $+3eV$ from the diffraction condition . The inset shows the fit in logarithmic scale for the diffraction condition.

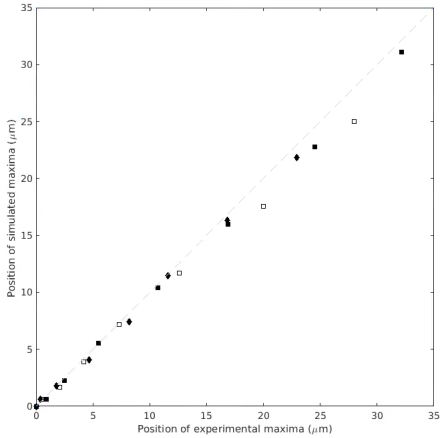

Figure 5. Comparison between fitted spatial displacement for experimental data and simulated cases. (Filled diamonds) Si (400) $100\mu m$ in FBD geometry, (filled squares) C (400) $220\mu m$ in FBD geometry and (empty squares) C (022) $220\mu m$ in FLD geometry. Dash line represents a perfect match between experiment and simulation.

6. OUTLOOK

We have present the dependence of the forward diffracted beam with the transverse direction to diffraction. As mentioned along the proceeding, this forward diffraction dependence is related to the spatio-temporal coupling. In the case of thin crystals as the one shown for both diamond and silicon the transverse displacement relates to tens of femtosecond. In other compounds with higher diffraction coefficient as Ge, InSb, GaAs the effect happens in thinner crystals with less than 10 μm thicknesses. Temporally these thicknesses relate to times around the femtosecond.

The spatio-temporal coupling depends highly of the perfection crystalline structure. This means that in the case of slightly strain crystals the echoes will depend of the different d spacing between the planes. Which could produce a broadening of the bandwidth appreciable in the echoes position and intensities.

ACKNOWLEDGMENTS

We would like to thank MicroXAS and the Swiss Light Source for supporting this research idea with beamtime. We would like to thank the NanoMAX beamline at MAX IV (Lund University) and the Instruments FXE and MID of the Eu XFEL GmbH facility for support to this work. One of us would like to thank Magnus H. Colliander, Steven van Petegem and Maxime Dupraz for the discussion in relation to the experiment.

REFERENCES

[1] Glownia, J. M., Cryan, J., Andreasson, J., Belkacem, A., Berrah, N., Blaga, C. I., Bostedt, C., Bozek, J., DiMauro, L. F., Fang, L., Frisch, J., Gessner, O., Ghr, M., Hajdu, J., Hertlein, M. P., Hoener, M., Huang, G., Kornilov, O., Marangos, J. P., March, A. M., McFarland, B. K., Merdji, H., Petrovic, V. S., Raman, C., Ray, D., Reis, D. A., Trigo, M., White, J. L., White, W., Wilcox, R., Young, L., Coffee, R. N., and Bucksbaum, P. H., "Time-resolved pump-probe experiments at the lcls," *Opt. Express* **18**, 17620 (2010).

[2] Tavares, P. F., Al-Dmour, E., Andersson, A., Cullinan, F., Jensen, B. N., Olsson, D., Olsson, D. K., Sjostrom, M., Tarawneh, H., Thorin, S., and Vorozhtsov, A., "Commissioning and first-year operational results of the max iv 3 gev ring," *J. Synchrotron Rad.* **25**, 1291–1316 (2018).

[3] Saldin, E. L., Schneidmiller, E. A., Shvyd'ko, Y. V., and Yurkov, M. V., "X-ray fel with a mev bandwidth," *Nucl. Instrum. Methods Phys. Res., Sect. A* **475**, 357–362 (2001).

[4] Geloni, G., Kocharyan, V., and Saldin, E., "Scheme for generation of highly monochromatic x-rays from a baseline xfel undulator," *DESY report* **10**, 053 (2010).

[5] Amann, J., Berg, W., Blank, V., Decker, F.-J., Ding, Y., Emma, P., Feng, Y., Frisch, J., Fritz, D., Hastings, J., Huang, Z., Krzywinski, J.and Lindberg, R., Loos, H., Lutman, A., Nuhn, H.-D., Ratner, D., Rzepiela, J., Shu, D., Shvyd'ko, Y., Spampinati, S., Stoupin, S., Terentyev, S., Trakhtenberg, E., Walz, D., Welch, J., Wu, J., Zholents, A., and Zhu, D., "Demonstration of self-seeding in a hard-x-ray free-electron laser," *Nature Photonics* **6**, 693–698 (2012).

[6] Villanueva-Perez, P., Pedrini, B., Mokso, R., Vagovic, P., Guzenko, V. A., Leake, S. J., Willmott, P. R., Oberta, P., David, C., Chapman, H. N., , and Stampanoni, M., "Hard x-ray multi-projection imaging for single-shot approaches," *Optica* **5**, 1521–1524 (2018).

[7] Rodriguez-Fernandez, A., Esposito, V., Sanchez, D. F., Finkelstein, K. D., Juranic, P., Staub, U., Grolimund, D., Reiche, S., and Pedrini, B., "Spatial displacement of forward-diffracted x-ray beams by perfect crystals," *Acta Cryst. A* **74**, 75 (2018).

[8] Batterman, B. and Cole, H., "Dynamical diffraction of x-rays by perfect crystals," *Reviews of Modern Physics* **36**, 681–717 (1964).

[9] Zachariasen, W. H., [*Theory of X-ray Diffraction in Crystals*], Dover Publications, INC, New York (1945).

[10] Shvydko, Y. and Lindberg, R., "Spatiotemporal response of crystals in x-ray bragg diffraction," *Phys. Rev. ST Accel. Beams* **15**, 100702 (2012).

[11] Bushuev, V. A., "Diffraction of x-ray free-electron laser femtosecond pulses on single crystals in the bragg and laue geometry," *J. Synchrotron Rad.* **15**, 495–505 (2008).

[12] Bushuev, V. A. and Samoylova, L., "Influence of diffraction in crystals on the coherence properties of x-ray free-electron laser pulses," *Crystall. Reports* **56**, 819–827 (2011).

[13] Bushuev, V. A. and Oreshko, A. P., "Diffraction reflection of x-ray with a two-dimensionally bounded wavefront from perfect crystals," *J. Surf. Investi. X-ray, Synchrotron and Neutron Tech.* **1**, 240–246 (2007).